Journal of Inorganic and Organometallic Polymers and Materials
https://doi.org/10.1007/s10904-026-04249-1

RESEARCH

Facile Synthesis of Iron-Based MIL-101 Metal-Organic Framework as a Potential Hydrogen Storage Material

Keaoleboga Mosupi[1] · Christophe A. Ndamyabera[1] · Mike Masukume[2] · Nicholas M. Musyoka[3] · Henrietta W. Langmi[1]

Received: 7 October 2025 / Accepted: 12 March 2026

Abstract

Conventional approaches for metal-organic framework synthesis have shortcomings that may be circumvented through unconventional approaches, which offer fast reactions and scale-up opportunities. This work reports the successful preparation of iron-based MIL-101 utilizing unconventional precursors: iron extracted from acid mine water and terephthalic acid derived from waste polyethylene terephthalate. Three methods were employed including conventional solvothermal, unconventional microwave-assisted and unconventional sonochemical-assisted synthesis and the resulting Fe-MIL-101 was evaluated as an adsorbent for hydrogen. Unconventional synthesis drastically reduced synthesis duration from 20 h (solvothermal) to 4 h (sonochemical-assisted) and 2 h (microwave-assisted). The prepared materials displayed comparable surface areas, with the sample from microwave-assisted synthesis exhibiting a surface area of 512 $m^2\ g^{-1}$ while that from sonochemical and conventional solvothermal methods exhibited surface areas of 702 and 717 $m^2\ g^{-1}$, respectively. Correspondingly, the highest hydrogen uptake (1.03 wt% at 1 bar, 77 K) was attained for the solvothermal Fe-MIL-101. The feasibility of synthesizing Fe-MIL-101 holistically from these specific waste sources using unconventional methods, with an advantage of shortened reaction times, has been proven in this study.

✉ Nicholas M. Musyoka
nicholas.musyoka@nottingham.edu.cn

✉ Henrietta W. Langmi
Henrietta.Langmi@up.ac.za

[1] Department of Chemistry, University of Pretoria, Private Bag X20, Hatfield 0028, South Africa

[2] Centre for Nanostructures and Advanced Materials, Chemical Cluster, Council for Scientific and Industrial Research (CSIR), Pretoria 0001, South Africa

[3] Nottingham Ningbo China Beacons of Excellence Research and Innovation Institute, University of Nottingham Ningbo China, Ningbo 315100, PR China

Published online: 24 March 2026

Graphical Abstract

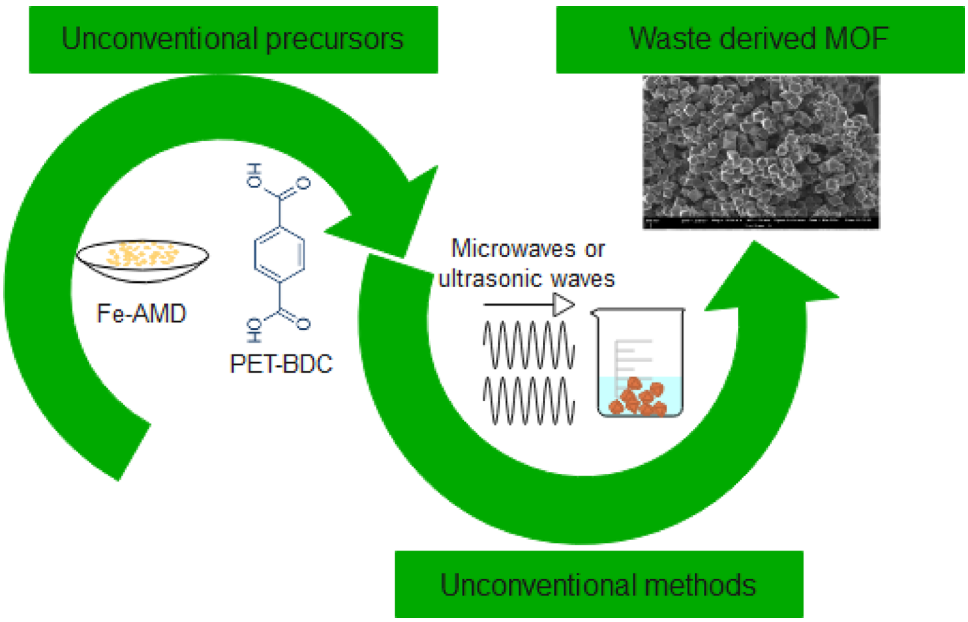

A drive towards sustainable synthesis of metal-organic frameworks as potential gas storage materials.

Keywords MIL-101 · Unconventional synthesis · Acid mine drainage · Polyethylene terephthalate · Hydrogen storage

1 Introduction

Metal-organic frameworks (MOFs) are a class of highly ordered crystalline compounds characterized by accessible voids of various shapes and sizes. They are known to possess unusually high specific surface areas and large pore volumes. The accessible voids are capable of ensnaring molecules of different sizes for various purposes. MOFs have been used in different applications such as heterogeneous catalysis [1–4], gas storage and separation [5–7]. Since hydrogen is considered as a good energy carrier there is a growing need to use MOFs as adsorbents for this gas. A few studies have reported on hydrogen storage in iron-based-MOFs. Hydrogen uptake of 5.1 wt% was reported for Fe-MIL-101 when the adsorption isotherm was recorded at 77 K and up to 100 bar pressure [8]. Anbia et al. obtained 0.3 mmol/g hydrogen uptake for Fe-MOF-235 which exhibited a surface area of 974 $m^2\ g^{-1}$ [5]. Fe-BTT (BTT^{3+} = 1,3,5-benzenetristetrazolate) with a surface area of 2010 $m^2\ g^{-1}$ and hydrogen uptake of 1.1 wt% at 100 bar and 298 K was also reported [9]. Although MOF materials possess good attributes, their industrial application is moving at a snail's pace. Use of enormous quantities of corrosive solvents, high energy demands with extended reaction times, and costly precursors are the biggest stumbling blocks to industrialization of these materials. The conventional synthesis, which requires pressure-sealed vessels, that are chemically and thermally resistant and normally in use for several days, adds to the delayed industrial application of MOFs.

Unconventional methods such as microwave-assisted synthesis provide a better alternative because of many benefits such as low reaction temperatures, fast synthesis times, uniform small crystals of the MOF and high yields. The working principle of microwave-assisted synthesis is based on interactions between charged particles (polar solvents and/or ions in solution) and electromagnetic waves. This method was employed for the synthesis of small crystals (200 nm) of Fe-MIL-101 which were used for drug delivery and imaging [10]. A comparison of conventional solvothermal and unconventional microwave synthesis of Fe-MIL-88 A was performed via computational methods and showed that the microwave method affords small crystals (< 100 nm) and has accelerated reaction rates [11]. The "breathing" effect of Fe-MIL-88B and Fe-MIL-88B-NH_2 was studied using the microwave method [12].

While on a quest to find better synthesis methods for industrial applications, sonochemical reaction has garnered a great interest in tailoring iron-based MOFs. Contrary to microwave, this method induces cavitation on liquids which upon reaching their critical size, they burst, emitting energy with heating and cooling rates of greater than 10^{10} K s^{-1}. Ultrasound does not interact with the molecules directly, it is the energy delivered by ultrasound-induced cavitation

that results in a very rapid synthesis reaction. This method is advantageous due to the fast reaction rates and the avoidance of high-pressure withstanding equipment [13, 14]. This method has been used to prepare Fe-MIL-53 and Fe-MIL-88 A yielding small highly crystalline particles at significantly reduced reaction times (2 h) [15, 16]. Several other unconventional methods have been reported for the synthesis of various MOFs [17–20].

Although unconventional methods contribute a fair share towards industrialization of MOFs, there is still a need to find cost effective and environmentally friendly precursors. The utilization of waste materials to create value-added products in chemistry represents a sustainable approach to resource management and environmental protection. Depolymerization of polyethylene terephthalate (PET) waste into an organic linker benzene-1,4-dicarboxylic acid (H_2BDC), has been widely used for the preparation of various MOFs and has afforded materials of similar quality to commercial linkers. Several MOFs, i.e., Fe-MIL-101, Cr-MIL-101, Fe-MIL-53, Fe-MIL-88B and Zr-UiO-66 were prepared using PET-derived H_2BDC (PET-BDC) with great properties for various applications [21–23]. One-pot solvothermal synthesis of Fe-MIL-88B and PET depolymerization in the presence of water and methanol, yielded Fe-MIL-88B crystals and unreacted H_2BDC [21]. Several other studies have employed the use of H_2BDC to generate various types of MOF [24–27]. These studies majorly employed the hydrolysis depolymerization technique which proves to be efficient for depolymerization of PET. Dyosiba et al. further extended the study to various source of organic linker such as food trays, colored (brown and green) bottles for the synthesis of Zr-MOFs [23]. Although the quality of the extracted H_2BDC was low as per acid test, the derived MOFs displayed reasonable surface areas.

In addition to repurposing waste PET, metals can be recovered from waste feedstock such as battery waste, coal flyash, and mine water drainage [28–31]. Acid mine drainage (AMD) is a major environmental problem arising from sulfide mineral mining activities. During mining activities, sulfide-bearing minerals such as pyrite are oxidized by air and water, which in turn produces sulfuric acid. The acid lowers the pH value of water which then dissolves heavy metals from the exposed rocks, contaminating the water even further [32]. The resulting highly acidic and metal containing water flows from open mines into the surrounding areas, which lead to long-term ecological effects. This waste can be neutralized through neutralizing agents such as lime or can be recycled and metals recovered for repurposing. Metals can be recovered through selective precipitation as hydroxides/oxyhydroxides by carefully adjusting the pH using neutralizing agents [31]. Seo et al. performed sequential selective precipitation of Fe, Al and Mn from coal acid mine water. The recovery of oxidized iron (Fe^{2+} to Fe^{3+}) was at 99% when pH was maintained at 3.5 [33]. In another study, 82% recovery of iron as iron hydroxide/oxyhydroxide was obtained with pH set at 3.7 [31]. Several other studies have shown good recovery rate of iron from AMD using selective precipitation via pH adjustment [34–36]. This study demonstrates the beneficiation of PET and AMD into a value-added product using microwave-assisted synthesis and sonochemical-assisted synthesis, and it evaluates the hydrogen storage capacity of the synthesized Fe-MIL-101. To the best of our knowledge, Fe-MIL-101 has not been previously prepared using microwave-assisted or sonochemical-assisted synthesis while employing holistic unconventional feedstock consisting of Fe-AMD and PET-BDC.

2 Experimental

2.1 Iron extraction

The oxidation of Fe^{2+} to Fe^{3+} in 1000 mL of AMD was performed by adding 30 mL of 30% H_2O_2. The solution was then stirred for 1.5 h at room temperature. Fe^{3+} was precipitated by dropwise addition of NaOH (4 M) to pH of 3.5 and it was agitated for 0.5 h. The resulting solid was vacuum filtered and washed with 1000 mL H_2O, and conventionally dried at 100 °C overnight.

2.2 Ligand Extraction

The ligand (H_2BDC) was extracted by depolymerizing waste PET. This was performed according to the method described by Dyosiba et al. with slight adjustments [37]. 37.5 g of flakes of PET, 37.5 mL of ethylene glycol, and 90 mL of deionized water were introduced into a 150 mL Teflon-lined stainless-steel autoclave. The mixture was heated to 210 °C and maintained at this temperature for 8 h under autogenous pressure. Upon completion, the solid product was recovered by centrifugation, washed twice with ethanol to remove impurities, and subsequently dried at 100 °C overnight. The resulting product was then utilized as an organic linker in the synthesis of Fe-MIL-101.

2.3 Solvothermal Synthesis

The extracted AMD iron salt (0.6655 g) was converted to $FeCl_3$ by dissolving in HCl (5 mL) at 70 °C. PET-derived BDC (0.4462 g) was added to dimethylformamide (DMF, 50 mL) and dissolved by ultrasonication. Then the iron salt solution was combined with PET-derived BDC solution and ultrasonicated for 0.5 h. The yellowish mixture was poured

into a Teflon cup in an autoclave and heated to 110 °C for 20 h. The brown orange precipitate was collected by centrifugation and washed thrice using DMF (50 mL ×3) followed by washing with ethanol three times (50 mL ×3). The sample was activated by heating at 60 °C in vacuum overnight. The product is denoted as Solvo-MIL-101.

2.4 Microwave Synthesis

A similar procedure to the solvothermal synthesis was followed with a minor change in organic linker solution where DMF (25 mL) and ethanol (25 mL) were used. The DMF/ethanol mixture aims to provide the solvent environment necessary to achieve reproducible, high-quality MOFs under rapid, energy-intensive synthesis conditions. Here, the organic linker and iron solution was transferred to a 100 mL four-neck round bottom flask and placed in a microwave reactor with power set at 250 W and heated to 80 °C for 2 h. The washing and activation procedure of the solvothermal process was adopted. The product is denoted as Micro-MIL-101.

2.5 Sonochemical Synthesis

A similar procedure to the microwave synthesis was followed, where the yellow solution was transferred to a 100 mL four-neck round bottom flask and placed in the reactor and continuous ultrasound probe set at 80% power for 4 h. A similar washing and activation procedure to that of the solvothermal process was followed. The product is denoted as Sono-MIL-101.

2.6 Characterization

Elemental composition of AMD was confirmed using inductively coupled plasma optical emission spectroscopy (ICP-OES, PerkinElmer Optima 2100 DV). The crystalline and/or amorphous phases of the synthesized materials were identified by powder X-ray diffraction (PXRD, Rigaku Ultima IV diffractometer) equipped with Ni-filtered Cu-Kα radiation (λ = 0.154 nm), scanned over a 2θ range of 5° to 80° at a rate of 0.1° s^{-1}. Fourier transform infrared (FTIR, JASCO FT/IR-4X spectrometer) spectra of the MOFs were recorded within the 4000–450 cm^{-1} region at a resolution of 16 cm^{-1}, with background spectra collected preceding sample analysis. Field emission scanning electron microscope (FE-SEM, JEOL JSM-7500 F) was used to determine the morphology of the prepared samples. Thermal stability of the material was tested using a Q500 analyzer (TA Instruments) TGA, under a nitrogen atmosphere. Each sample was loaded into an alumina crucible and heated from 0 °C to 900 °C at a rate of 10 °C min^{-1}. The Brunauer–Emmett–Teller (BET) specific surface area and porosity were determined using a Quantachrome Autosorb iQ instrument at 77 K, over a relative pressure (p/p_o) range of 0 to 1. Pore size distribution and pore volume were calculated using the Horvath-Kawazoe (H-K) model. Micropore surface area and micropore volume were determined using t-plot. Hydrogen adsorption isotherms were measured at 77 K up to 1 bar using Micromeritics ASAP 2020 HD, with ultra-high purity hydrogen gas (99.999%).

3 Results and Discussion

3.1 Viability of Using Wastes as Precursors

3.1.1 PET-Derived H_2BDC

The successful extraction of H_2BDC from PET waste was confirmed by both PXRD and FTIR spectroscopy. The PXRD pattern of extracted H_2BDC with reflection peaks at 2θ = 17.69, 25.45, 28.09, 30.07, 40.07° (Fig. 1a) is similar to the commercial and literature reported samples [37]. No impurities were observed and the H_2BDC product was highly crystalline. Figure 1b shows FTIR spectrum of the extracted H_2BDC with prominent distinctive signals attributed to vibrations of C=O, COO^- and OH. The benzene ring of terephthalic acid is confirmed by the vibration peak of C-H at 723 cm^{-1} and the bending of O–H wagging vibration at 929 cm^{-1}. The COO^- and C=O stretching bands are observable at 1278, 1423 and 1675 cm^{-1}. The broad peak at 2834 cm^{-1} represents the stretching vibration of OH group.

3.1.2 Iron-Derived AMD

Quantitative analysis of metals present in raw AMD was performed using ICP-MS. The raw AMD sample had a high amount of Fe (808 mg L^{-1}), followed by Ca, Mg, Al and Mn (Table 1). Other metals including Cu, Cr, Pb and As were present only in trace amounts. This revealed that the AMD was iron-rich. The amount of Fe was high enough to be extracted for use in synthesizing Fe-MOFs. The PXRD pattern of extracted Fe-AMD is shown in Fig. 1c, where β-FeOOH peaks are observed at 2θ = 7.54 and 35.68° while the broad peak at 2θ = 15.87° is assigned to the γ-FeOOH. This confirmed that Fe was successfully extracted from AMD by the precipitation method with pH control. The extracted material is mostly amorphous as indicated by broad diffraction peaks. SEM-EDS (Fig. 1d; Table 2) was used to determine the elemental composition of the extracted iron. The results revealed the main presence of iron and trace amount of aluminum which may have originated either from the sample itself or the sample holder used

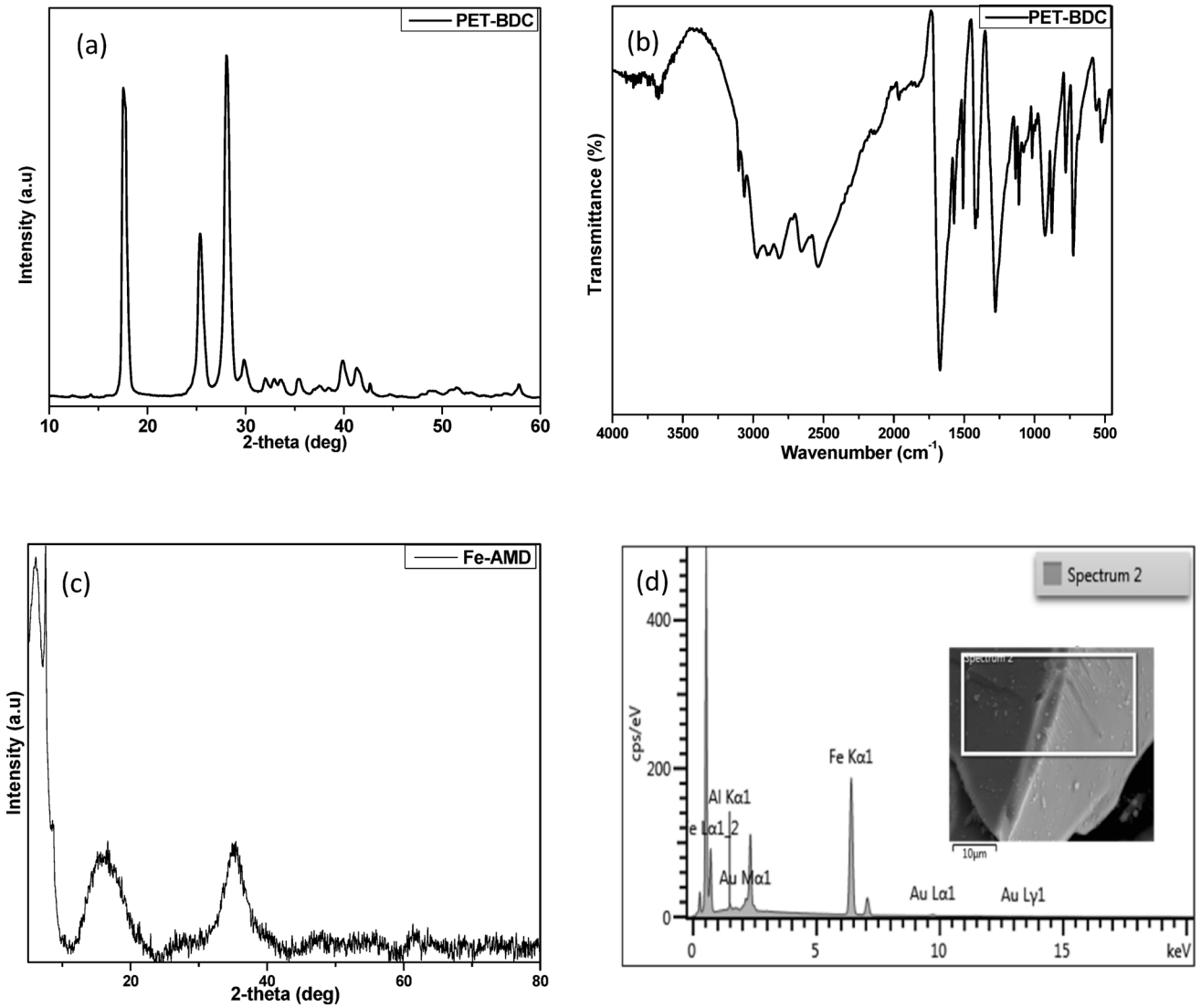

Fig. 1 **a** PXRD pattern and **b** FTIR spectrum of PET extracted H_2BDC, **c** PXRD pattern of extracted iron from AMD and **d** SEM-EDS (point and ID) of iron extracted from AMD

Table 1 Elemental composition of raw AMD

Identified element	Amount identified (mg L^{-1})
Ca	101
Mg	94
Al	67
Fe	808
Mn	18
Zn	1.83
As	0.055
Pb	0.025
Cr	< 0.125
Cu	< 0.050

Table 2 Metal composition of iron extracted from AMD

Element	Wt%	Wt% Sigma	Atomic %
Al	1.62	0.03	3.29
Fe	98.38	0.03	96.71
Total:	100.00		100.00

in the analysis. Nevertheless, the successful extraction of iron is further confirmed.

3.2 Fe-MIL-101 Synthesized from Different Methods

3.2.1 Phase and Morphology Confirmation

The AMD-derived Fe and PET-derived H_2BDC were used to synthesize Fe-MIL-101. Figure 2, shows the PXRD patterns of Fe-MIL-101 synthesized using solvothermal,

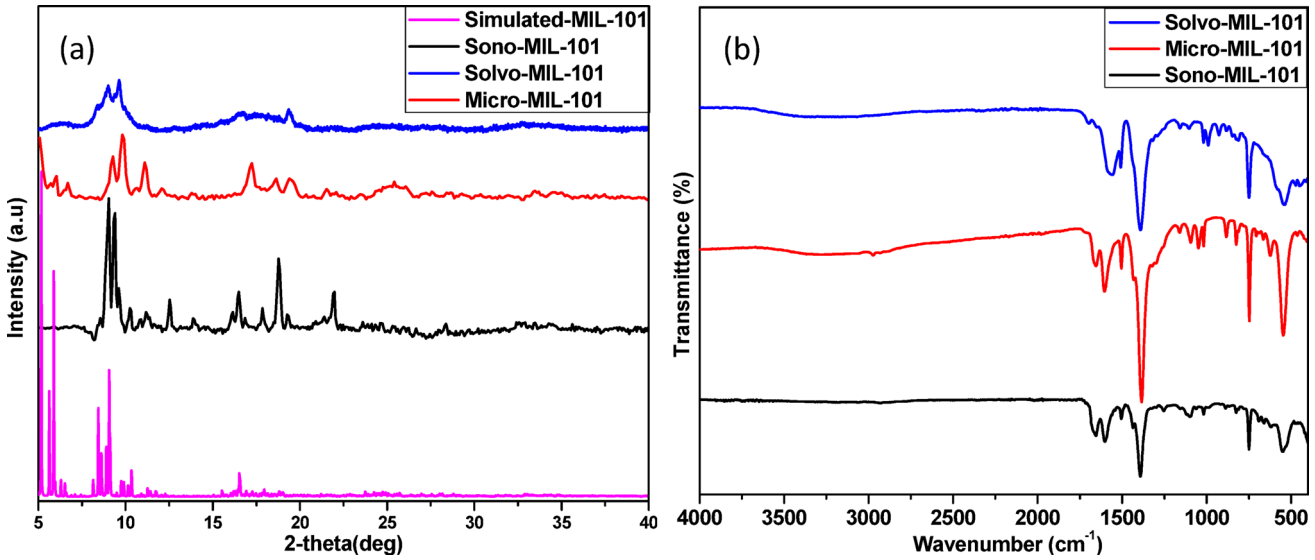

Fig. 2 **a** PXRD patterns and **b** FTIR spectra of as-prepared Fe-MIL-101

microwave-assisted and sonochemical-assisted routes. The patterns for microwave-assisted and sonochemical-assisted prepared Fe-MIL-101 MOFs showed distinctive peaks at 2θ values of 8.39 and 10.3°. Further peaks were observed at 12.58, 18.86, 19.34 and 22°, which are characteristic of trinucleated-transition metal-based MOFs (Fig. 2a). The peaks represent (002), (100), (101), (103), (202, and (211) planes, in good agreement with earlier reports [38, 39]. The patterns of the as-prepared materials correspond to the simulated Cr-MIL-101 pattern, with a slight shift of peaks to higher 2-theta values attributed to the different metal centres consistent with lattice contraction. The Cr-MIL-101 and Fe-MIL-101 are isostructural hence the use of Cr-MIL-101 PXRD pattern. VESTA software was used to generate the patterns from a CIF file published by Lebedev et al. [40]. The absence of the peaks between 5 and 7° for the Solvo-MIL-101 and Sono-MIL-101 is also consistent with the literature [38, 39]. The high crystallinity of the MOFs from microwave-assisted and sonochemical-assisted synthesis is confirmed by the high intensity and extremely small regions under the peaks on the XRD patterns. The solvothermally synthesized material displayed relatively weak broad diffraction peaks (at 2θ values of 8.39, 10.3 and 18.5°) which shows a slight decrease in crystallinity. Other studies have shown relative less crystalline samples of MIL-101 [41, 42]. This confirms that Fe-MIL-101 materials were successfully prepared by the three methods though with varied degrees of crystallinity.

The molecular structure and functional groups of the MOFs were examined using FTIR-spectroscopy as displayed in Fig. 2b. The absence of a broad peak at 3330 cm^{-1} signifies the successful evacuation of guest molecules in the cavities of all the MOFs. The successful synthesis of the MOFs is confirmed by characteristic peaks at 550, 748, 1096, 1398, 1505, 1659 cm^{-1} in the case of the solvothermally synthesized Fe-MIL-101. The peak at 550 cm^{-1} confirms the stretching vibrations of Fe–O bond. The peaks at 748, 1398, 1505 and 1659 cm^{-1} confirm the presence of carboxylate ligand. The 748 cm^{-1} peak is assigned to C-H bending vibrations, 1398 and 1505 cm^{-1} are assigned to the C=O symmetric and asymmetric vibrations while the peak at 1659 cm^{-1} indicates the C–O stretching bands. The stretching vibration ascribed to C–O–Fe is represented by a band at 1096 cm^{-1}. For microwave-assisted and sonochemical-assisted Fe-MIL-101, these characteristic bands were also observed at similar positions. Therefore, the FTIR results are in agreement with the observation from PXRD that Fe-MIL-101 was indeed formed from each of the synthesis routes.

Figure 3 presents the morphology of the MOFs synthesized by solvothermal, microwave-assisted and sonochemical-assisted approaches. All methods show well-faceted crystals with octahedral morphology and smooth surfaces, associated with Fe-MIL-101, corroborating the results from PXRD and FTIR spectroscopy that Fe-MIL-101 was synthesized. The surface morphology is similar to the typical crystalline and porous iron-based MOFs that have been reported [42, 43]. The Micro-MIL-101 displayed exceptional homogeneity, which is attributed to the fast nucleation and good phase selectivity brought about by the microwaves. The fast crystallization contributes immensely to the narrow particle size and uniformity of Micro-MIL-101. The small particle size (75–300 nm) could contribute to the external surface area of the material. The MOF from sonochemical-assisted synthesis also displayed reasonable uniformity. Meanwhile, the particle was larger and less uniform for Solvo-MIL-101

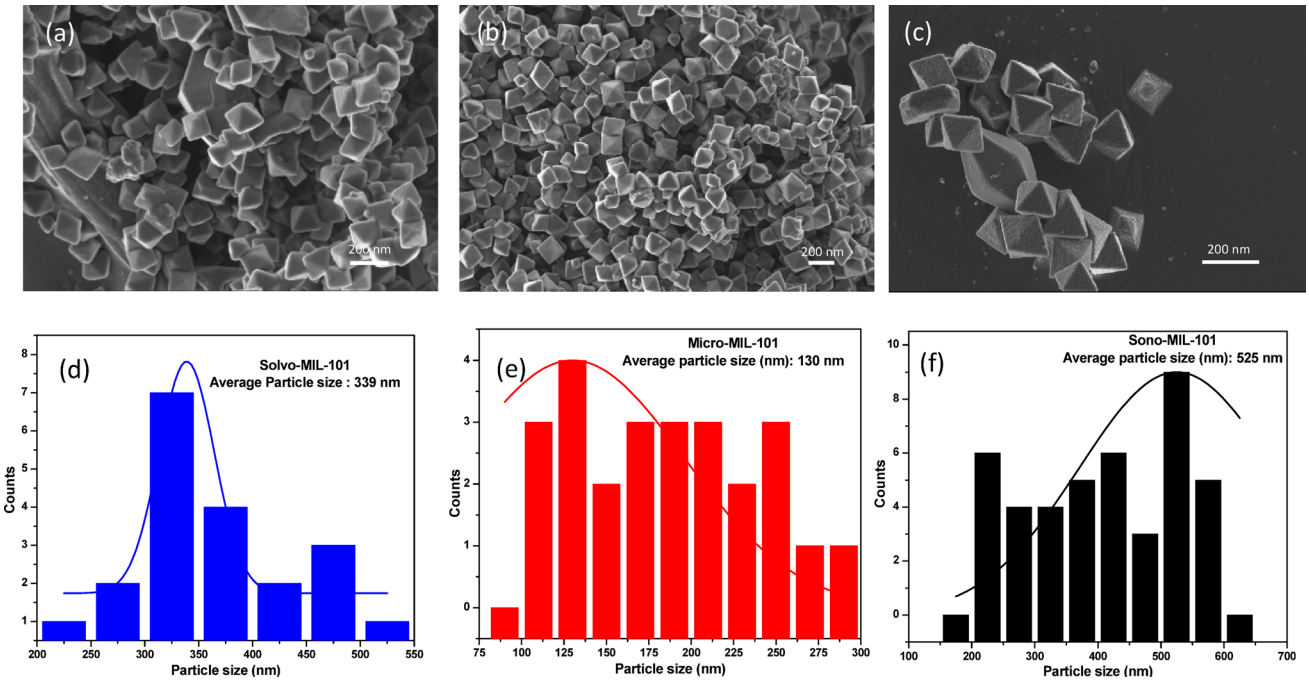

Fig. 3 SEM images of **a** Solvo-MIL-101 **b** Micro-MIL-101 and **c** Sono-MIL-101 and particle size distribution **d** Solvo-MIL-101 **e** Micro-MIL-101 and **f** Sono-MIL-101

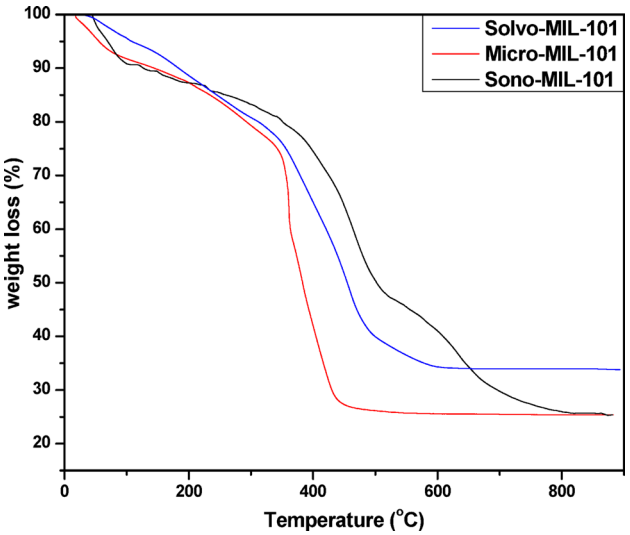

Fig. 4 TGA plots of synthesized Fe-MIL-101

(200–500 nm) and Sono-MIL-101 (150–650 nm). The reported particle sizes are in line with previously reported values [44–46]. Overall, structural and morphological characterization of the MOFs from the three different methods employed in this study demonstrates the feasibility of using a combination of Fe-AMD and PET-H_2BDC to synthesize Fe-MIL-101.

3.2.2 Thermal Stability

Thermogravimetric analysis (TGA) was used for the assessment of the thermal stability of the prepared samples. The TGA profiles of the MOF materials derived from Fe-AMD and PET-BDC utilizing unconventional methods are displayed in Fig. 4. The initial weight loss occurring between approximately 30–200 °C accounts for a 10% reduction in weight. This is attributed to the gradual loss of pore-trapped solvent molecules as well as those bound to the iron atoms. The second weight loss between 300 and 580 °C corresponds to the breakdown of the Fe-MIL-101 framework and degradation of the carboxylate moiety. The sharper, well-defined framework decomposition step for Micro-MIL-101 indicates a more effective removal of trapped solvent molecules. The third weight loss for Solvo-MIL-101 and Sono-MIL-101 at temperatures above 580 °C can be attributed to the loss of CO_2 due to decarboxylation of the organic linker [47]. Therefore, the MOFs are generally thermally stable up to about 300 °C.

3.2.3 Textural Properties and Hydrogen Uptake

Textural properties of the prepared materials were determined using nitrogen at 77 K, and the N_2 sorption isotherms and pore size distribution are shown in Fig. 5a and c. All the synthesized MOFs displayed a classical IUPAC Type I (a) adsorption isotherm which is representative of microporous materials. This IUPAC Type has been previously reported

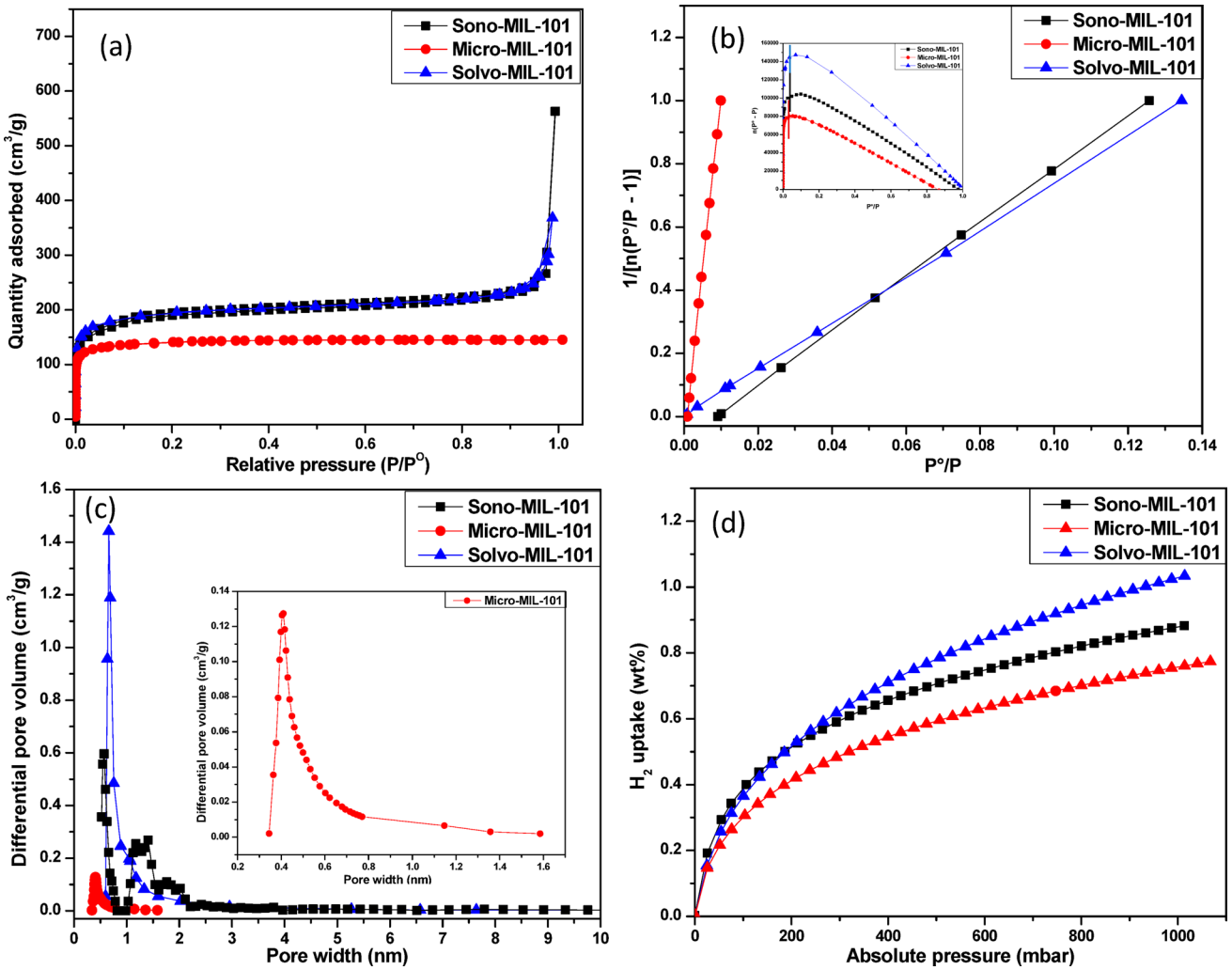

Fig. 5 **a** N_2 sorption isotherms at 77 K, **b** Linear BET plot in the finally selected pressure range (Normalized, insert (Plot of the term n (P^O - P) vs. P/P^O)), **c** pore size distribution and **d** hydrogen adsorption isotherms at 77 K for synthesized Fe-MIL-101

Table 3 Textural properties and hydrogen uptakes of prepared Fe-MIL-101

Sample name	BET Specific surface area ($m^2\ g^{-1}$)	BET micropore surface area ($m^2\ g^{-1}$)	Pore size (nm)	Pore volume ($cm^3\ g^{-1}$)	Micropore volume ($cm^3\ g^{-1}$)	H_2 uptake at 1 bar (wt%)
Micro-MIL-101	512	417	1.75	0.22	0.18	0.77
Sono-MIL-101	702	477	1.76	0.39	0.12	0.90
Solvo-MIL-101	717	505	1.81	0.60	0.23	1.03

for MIL-101(Fe) [48, 49]. The steep gas uptake at lower partial pressure signifies the presence of micropores in the material (evident on all samples). The BET surface area and pore volume of the prepared materials are relatively comparable (Table 3). The low surface areas of these materials may be attributed to the possibility of unreacted precursors in the pores of the prepared MOFs and/or partial collapse of the pores thus reducing the accessible surface area. To determine the BET surface area a linear plot must be identified. From this linear plot, a monolayer capacity can be determined then multiplied with the Avogrado's number and cross-sectional area of the adsorbate which will then give BET surface area. Figure 5c displays normalized linear plots of the prepared samples. The linear plot is often determined from the plot of $n(P^0 - P)$ vs. P/P^0 (insert) which determines the upper relative pressure limit (signified with lines on the plot) for the linear plot. The determined surface areas of the prepared MOFs are in line with the criteria outlined by Rouquerol and Llewellyn [50]. Dong et al. prepared Fe-MIL-101 via conventional electric heating and microwave-assisted synthesis [51]. The microwave-assisted samples showed improvement in surface area (383 $m^2\ g^{-1}$)

compared to the conventional heating materials (309 m^2 g^{-1}). In another study, microwave-assisted preparation of Fe-MIL-101 was conducted and the material displayed a high surface area of 1693 m^2 g^{-1} [52]. The pore size distribution calculated via H-K method showed that all the three MOF materials are dominated by pores with pore sizes below 2 nm.

The hydrogen adsorption capacity of the prepared MOFs was measured at cryo-temperature (77 K) and 1 bar. Figure 5e displays the hydrogen adsorption isotherms for all the Fe-MIL-101 samples. The obtained hydrogen uptakes of 0.77, 0.90 and 1.03 wt% at 1 bar and 77 K for Micro-MIL-101, Sono-MIL-101 and Solvo-MIL-101, respectively are comparable to values reported in literature for MOFs at these conditions with correspondingly similar surface areas. For instance, IRMOF-1 (BET surface area = 520 m^2 g^{-1}) and Co-Cu-BTC (BET surface area = 822 m^2 g^{-1}) have been reported to adsorb 0.97 and 1.12 wt% hydrogen, respectively [53, 54]. A recent work reported hydrogen uptake of 1.0 wt% for a sustainably synthesized Fe-MIL-100 material, which was correlated with its BET surface area [55]. These reported hydrogen uptake values are in the range of the hydrogen uptake values recorded for the Fe-MIL-101 samples in this work. Other work by Yuan et al. reported that PCN-61, with a BET surface area of 3000 m^2 g^{-1}, exhibited reversible hydrogen adsorption of 2.25 wt % at 77 K and 1 bar [56]. In another study, a microporous iron-based MOF, Fe-BTT with a high BET surface area and open Fe^{2+} cation sites displayed a hydrogen uptake of about 2.3 wt% at 1 bar and 77 K [9]. Evidently, Solvo-MIL-101 with the highest surface area exhibited the highest hydrogen uptake. The absence of saturation in the hydrogen adsorption isotherms at pressures up to 1 bar suggests that higher uptake capacities may be achievable at elevated pressures, as increased pressure would drive more hydrogen molecules into the material's pores [57]. These results demonstrate that the Fe-MIL-101 obtained from traditional solvothermal synthesis is superior over those obtained from unconventional sonochemical-assisted and microwave-assisted synthesis. Hydrogen adsorption on porous materials is mainly governed by weak van der Waals forces, which is highly dependent on temperature. Cryogenic temperatures (77 K) lower kinetic energy of H_2 which allows molecules to remain in MOF pores thus resulting in high adsorption capacities. Although adsorption data at higher temperatures were not collected in the present work, previous studies on MIL-101 and related MOFs consistently report a sharp reduction in hydrogen uptake with increasing temperature, attributed to relatively low adsorption enthalpies (typically 6–10 kJ mol^{-1}). This trend is consistent across MOFs with diverse structural features including high surface areas or open metal sites and is expected to be similar for the MOFs reported here [58–60].

4 Conclusions

Successful synthesis of Fe-MIL-101 was achieved from waste precursors including AMD and PET by unconventional and conventional methods. The extract from AMD was confirmed to contain predominantly iron. PXRD and FTIR spectra confirmed the successful extraction of H_2BDC linker from PET waste. Unconventional methods such as microwave-assisted and sonochemical-assisted synthesis were proven to reduce the long synthetic times (20 h) to 2 h and 4 h, respectively. The need for pressure withstanding equipment (Teflon cups and autoclaves) was eliminated by the unconventional methods, which utilized round bottom flasks. This sustainable synthesis pathway reduced the volume of corrosive solvent employed by utilizing 1 : 1 v/v ratio of ethanol and *N*, *N*-dimethylformamide. The resulting morphology of the MOF from the unconventional approaches was similar to the solvothermally prepared MOF but with smooth surface and uniform small particles (130 nm). The results obtained in this study show that the preparation of MOFs using unconventional techniques and precursors could serve as a basis for developing MOF-based materials that can satisfy a range of applications, including their potential use in hydrogen storage. Future studies will involve long-term recyclability testing and temperature- and pressure-dependent hydrogen uptake measurements.

Acknowledgements HWL and MM gratefully acknowledge funding from the MAST3RBoost project funded by the European Union (Call HORIZON-CL4-2021-RESILIENCE-01, Grant Agreement No: 101058574). HWL acknowledges the South African Research Chairs Initiative (SARChI) of the Department of Science and Innovation and the National Research Foundation (Grant Number: 2090155358). Also, NMM acknowledges financial support provided by the Nottingham Ningbo China Beacons of Excellence Research and Innovation Institute.

Author contributions Keaoleboga Mosupi: Formal analysis, Investigation, methodology, validation, visualization, writing – original draft. Christophe A. Ndamyabera: Project administration, formal analysis, writing – review & editing. Mike Masukume: Resources, writing – review & editing. Nicholas M. Musyoka: Conceptualization, methodology, funding acquisition, supervision, writing – review & editing. Henrietta W. Langmi: Conceptualization, supervision, funding acquisition, methodology, resources, project administration, writing –review & editing.

Funding Open access funding provided by University of Pretoria.

Data Availability The experimental data that supports the findings of this study will be available on request.

Declarations

Conflict of interest The authors declare no competing interests.

References

1. L. Jiang, X. Yuan, G. Zeng, J. Liang, Z. Wu, H. Wang, *Construction of an All-Solid-State Z-Scheme Photocatalyst Based on Graphite Carbon Nitride and its Enhancement to Catalytic Activity*, vol. 5 (Nano, Environmental Science, 2018), pp.599–615
2. L. Ai, C. Zhang, L. Li, J. Jiang, Iron terephthalate metal–organic framework: revealing the effective activation of hydrogen peroxide for the degradation of organic dye under visible light irradiation. Appl. Catal. B. **148**, 191–200 (2014)
3. K.G. Laurier, F. Vermoortele, R. Ameloot, D.E. De Vos, J. Hofkens, M.B. Roeffaers, Iron (III)-based metal–organic frameworks as visible light photocatalysts. J. Am. Chem. Soc. **135**, 14488–14491 (2013)
4. Y. Qin, M. Hao, Z. Ding, Z. Li, Pt@ MIL-101 (Fe) for efficient visible light initiated coproduction of benzimidazoles and hydrogen from the reaction between o-Phenylenediamines and alcohols. J. Catal. **410**, 156–163 (2022)
5. M. Anbia, V. Hoseini, S. Sheykhi, Sorption of methane, hydrogen and carbon dioxide on metal-organic framework, iron terephthalate (MOF-235). J. Ind. Eng. Chem. **18**, 1149–1152 (2012)
6. J.S. Lee, S.H. Jhung, J.W. Yoon, Y.K. Hwang, J.-S. Chang, Adsorption of methane on porous metal carboxylates. J. Ind. Eng. Chem. **15**, 674–676 (2009)
7. T.N. Tu, H.T. Nguyen, N.T. Tran, Tailoring the pore size and shape of the one-dimensional channels in iron-based MOFs for enhancing the methane storage capacity. Inorg. Chem. Front. **6**, 2441–2447 (2019)
8. D. Lupu, O. Ardelean, G. Blanita, G. Borodi, M.D. Lazar, A.R. Biris, C. Ioan, M. Mihet, I. Misan, G. Popeneciu, Synthesis and hydrogen adsorption properties of a new iron based porous metal-organic framework. Int. J. Hydrogen Energy **36**, 3586–3592 (2011)
9. K. Sumida, S. Horike, S.S. Kaye, Z.R. Herm, W.L. Queen, C.M. Brown, F. Grandjean, G.J. Long, A. Dailly, J.R. Long, Hydrogen storage and carbon dioxide capture in an iron-based sodalite-type metal–organic framework (Fe-BTT) discovered via high-throughput methods. Chem. Sci. **1**, 184–191 (2010)
10. K.M. Taylor-Pashow, J. Della Rocca, Z. Xie, S. Tran, W. Lin, Postsynthetic modifications of iron-carboxylate nanoscale metal–organic frameworks for imaging and drug delivery. J. Am. Chem. Soc. **131**, 14261–14263 (2009)
11. T. Chalati, P. Horcajada, R. Gref, P. Couvreur, C. Serre, Optimisation of the synthesis of MOF nanoparticles made of flexible porous iron fumarate MIL-88A. J. Mater. Chem. **21**, 2220–2227 (2011)
12. M. Ma, A. Bétard, I. Weber, N.S. Al-Hokbany, R.A. Fischer, N. Metzler-Nolte, Iron-based metal–organic frameworks MIL-88B and NH2-MIL-88B: high quality microwave synthesis and solvent-induced lattice "breathing." Crystal growth & design **13**, 2286–2291 (2013)
13. J.H. Bang, K.S. Suslick, Applications of ultrasound to the synthesis of nanostructured materials. Adv. Mater. **22**, 1039–1059 (2010)
14. C. Vaitsis, G. Sourkouni, C. Argirusis, Metal organic frameworks (MOFs) and ultrasound: a review. Ultrason. Sonochem. **52**, 106–119 (2019)
15. J.H. Lee, Y. Ahn, S.-Y. Kwak, Facile sonochemical synthesis of flexible Fe-based metal–organic frameworks and their efficient removal of organic contaminants from aqueous solutions. ACS Omega **7**, 23213–23222 (2022)
16. J. Amaro-Gahete, R. Klee, D. Esquivel, J.R. Ruiz, C. Jiménez-Sanchidrián, F.J. Romero-Salguero, Fast ultrasound-assisted synthesis of highly crystalline MIL-88A particles and their application as ethylene adsorbents. Ultrason. Sonochem. **50**, 59–66 (2019)
17. H. Hu, H. Xie, S. Liang, M. Yu, F. Liu, S. Deng, S. Wang, W. Xiao, C. Chen, Fabricating MOF-supported nonprecious metal nanocatalysts from the commercial metal dusts via a mechanochemistry-assisted sacrificial strategy. Inorg. Chem. **64**, 21674–21682 (2025)
18. K. Mosupi, M. Masukume, G. Weng, N.M. Musyoka, H.W. Langmi, Recent advances in Fe-based metal-organic frameworks: structural features, synthetic strategies and applications. Coord. Chem. Rev. **529**, 216467 (2025)
19. K. Mosupi, N.T. Mthembu, M. Masukume, N.M. Musyoka, H.W. Langmi, Synthesis of iron-based metal–organic frameworks and carbon derivatives via unconventional synthetic methods and waste precursors with potential for gas storage. Mater. Adv. (2025). https://doi.org/10.1039/d5ma00994d
20. J. Joseph, S. Iftekhar, V. Srivastava, Z. Fallah, E.N. Zare, M. Sillanpää, Iron-based metal-organic framework: synthesis, structure and current technologies for water reclamation with deep insight into framework integrity. Chemosphere **284**, 131171 (2021)
21. W.P. Deleu, I. Stassen, D. Jonckheere, R. Ameloot, D.E. De Vos, Waste PET (bottles) as a resource or substrate for MOF synthesis. J. Mater. Chem. A **4**, 9519–9525 (2016)
22. N.P. Makhanya, B. Oboirien, N. Musyoka, J. Ren, P. Ndungu, Evaluation of PET-derived metal organic frameworks (MOFs) for water adsorption and heat storage. J. Porous Mater. **30**, 387–401 (2023)
23. X. Dyosiba, J. Ren, N.M. Musyoka, H.W. Langmi, M. Mathe, M.S. Onyango, Feasibility of varied polyethylene terephthalate wastes as a linker source in metal–organic framework UiO-66 (Zr) synthesis. Ind. Eng. Chem. Res. **58**, 17010–17016 (2019)
24. F. Zhang, S. Chen, S. Nie, J. Luo, S. Lin, Y. Wang, H. Yang, Waste PET as a reactant for lanthanide MOF synthesis and application in sensing of picric acid. Polymers **11**, 2015 (2019)
25. D. Villarroel-Rocha, M.C. Bernini, J.J. Arroyo-Gómez, J. Villarroel-Rocha, K. Sapag, Synthesis of MOF-5 using terephthalic acid as a ligand obtained from polyethylene terephthalate (PET) waste and its test in CO2 adsorption. Braz. J. Chem. Eng. **39**, 949–959 (2022)
26. S.D. Farahani, J. Zolgharnein, Sulfate removal by barium-terephthalate MOF synthesized from recycled PET-waste using Doehlert design optimization. Inorg. Chem. Commun. **140**, 109388 (2022)
27. L. Karam, A. Miglio, S. Specchia, N. El Hassan, P. Massiani, J. Reboul, Pet waste as organic linker source for the sustainable

preparation of MOF-derived methane dry reforming catalysts. Mater. Adv. **2**, 2750–2758 (2021)
28. E. Perez, M.-L. Andre, R.N. Amador, F. Hyvrard, J. Borrini, M. Carboni, D. Meyer, Recovery of metals from simulant spent lithium-ion battery as organophosphonate coordination polymers in aqueous media. J. Hazard. Mater. **317**, 617–621 (2016)
29. K.M. Rambau, N.M. Musyoka, R. Panek, W. Franus, M. Wdowin, N. Manyala, Preparation of coal fly ash derived metal organic frameworks and their carbon derivatives. Mater. Today Commun. **27**, 102433 (2021)
30. V. Akinwekomi, J. Maree, V. Masindi, C. Zvinowanda, M.S. Osman, S. Foteinis, L. Mpenyana-Monyatsi, E. Chatzisymeon, Beneficiation of acid mine drainage (AMD): a viable option for the synthesis of goethite, hematite, magnetite, and gypsum–gearing towards a circular economy concept. Miner. Eng. **148**, 106204 (2020)
31. R. de Almeida Silva, M.P. Secco, R.T. Lermen, I.A.H. Schneider, G.E.N. Hidalgo, C.H. Sampaio, Optimizing the selective precipitation of iron to produce yellow pigment from acid mine drainage. Miner. Eng. **135**, 111–117 (2019)
32. A. Akcil, S. Koldas, Acid Mine Drainage (AMD): causes, treatment and case studies. J. Clean. Prod. **14**, 1139–1145 (2006)
33. E. Seo, Y. Cheong, G. Yim, K. Min, J. Geroni, Recovery of Fe, Al and Mn in acid coal mine drainage by sequential selective precipitation with control of pH. Catena **148**, 11–16 (2017)
34. R. de Almeida Silva, C.D. Castro, E.M. Vigânico, C.O. Petter, I.A.H. Schneider, Selective precipitation/UV production of magnetite particles obtained from the iron recovered from acid mine drainage. Miner. Eng. **29**, 22–27 (2012)
35. A. Roa, J. López, J.L. Cortina, Recovery of rare earth elements from acidic mine waters: a circular treatment scheme utilizing selective precipitation and ion exchange. Sep. Purif. Technol. **338**, 126525 (2024)
36. R. de Almeida Silva, J. Menezes, F.A. Lopes, A.P. Kirchheim, I.A.H. Schneider, Synthesis of a goethite pigment by selective precipitation of iron from acidic coal mine drainage. Mine Water Environ. **36**, 386–392 (2017)
37. X. Dyosiba, J. Ren, N.M. Musyoka, H.W. Langmi, M. Mathe, M.S. Onyango, Preparation of value-added metal-organic frameworks (MOFs) using waste PET bottles as source of acid linker. Sustain. Mater. Technol. **10**, 10–13 (2016)
38. Z. Li, X. Liu, W. Jin, Q. Hu, Y. Zhao, Adsorption behavior of arsenicals on MIL-101 (Fe): the role of arsenic chemical structures. J. Colloid Interface Sci. **554**, 692–704 (2019)
39. H. Hu, H. Zhang, Y. Chen, H. Ou, Enhanced photocatalysis using metal–organic framework MIL-101 (Fe) for organophosphate degradation in water. Environ. Sci. Pollut. Res. **26**, 24720–24732 (2019)
40. O. Lebedev, F. Millange, C. Serre, G. Van Tendeloo, G. Férey, First direct imaging of giant pores of the metal− organic framework MIL-101. Chem. Mater. **17**, 6525–6527 (2005)
41. A.D. Barbosa, D. Julião, D.M. Fernandes, A.F. Peixoto, C. Freire, B. de Castro, C.M. Granadeiro, S.S. Balula, L. Cunha-Silva, Catalytic performance and electrochemical behaviour of Metal–organic frameworks: MIL-101 (Fe) versus NH2-MIL-101 (Fe). Polyhedron **127**, 464–470 (2017)
42. H.T.M. Thanh, T.T.T. Phuong, P.T. Le Hang, T.T.T. Toan, T.N. Tuyen, T.X. Mau, D.Q. Khieu, Comparative study of Pb (II) adsorption onto MIL–101 and Fe–MIL–101 from aqueous solutions. J. Environ. Chem. Eng. **6**, 4093–4102 (2018)
43. Y. Jin, X. Mi, J. Qian, N. Ma, W. Dai, Modular construction of an MIL-101 (Fe)@ MIL-100 (Fe) dual-compartment nanoreactor and its boosted photocatalytic activity toward tetracycline. ACS Appl. Mater. Interfaces. **14**, 48285–48295 (2022)
44. Y.Q. Liu, C.G. Song, G. Ding, J. Yang, J.R. Wu, G. Wu, M.Z. Zhang, C. Song, L.P. Guo, J.C. Qin, High-performance functional Fe-MOF for removing aflatoxin B1 and other organic pollutants. Adv. Mater. Interfaces **9**, 2102480 (2022)
45. S.H. Ghoochani, A. Heshmati, H.A. Hosseini, M. Darroudi, Adsorption and photocatalytic properties of porphyrin loaded MIL-101 (Cr) in methylene blue degradation. Environ. Sci. Pollut. Res. **29**, 34406–34418 (2022)
46. A. Pangestu, W.W. Lestari, F.R. Wibowo, L. Larasati, Green electro-synthesized MIL-101 (Fe) and its aspirin detoxification performance compared to MOF-808. J. Inorg. Organomet. Polym. Mater. **32**, 1828–1839 (2022)
47. J. Tang, M. Yang, M. Yang, J. Wang, W. Dong, G. Wang, Heterogeneous Fe-MIL-101 catalysts for efficient one-pot four-component coupling synthesis of highly substituted pyrroles. New J. Chem. **39**, 4919–4923 (2015)
48. S. Xi, L. Gao, W. Yao, J. Huang, R. Chen, W. Wu, D. Xu, X. Dong, H. Wang, M. Gong, Study on the low-temperature and high-pressure hydrogen storage performance of MIL-101 (Cr)-filled type III tank. Int. J. Hydrog. Energy. **128**, 95–104 (2025)
49. C. Gecgel, U.B. Simsek, B. Gozmen, M. Turabik, Comparison of MIL-101 (Fe) and amine-functionalized MIL-101 (Fe) as photocatalysts for the removal of imidacloprid in aqueous solution. J. Iran. Chem. Soc. **16**, 1735–1748 (2019)
50. J. Rouquerol, P. Llewellyn, F. Rouquerol, *Is the BET equation applicable to microporous adsorbents? Studies in surface science and catalysis* (Elsevier, Amsterdam, 2007), pp.49–56
51. Y. Dong, T. Hu, M. Pudukudy, H. Su, L. Jiang, S. Shan, Q. Jia, Influence of microwave-assisted synthesis on the structural and textural properties of mesoporous MIL-101 (Fe) and NH2-MIL-101 (Fe) for enhanced tetracycline adsorption. Mater. Chem. Phys. **251**, 123060 (2020)
52. A. Franco, S.R. Balestra, S. Hamad, C. Carrillo-Carrión, Full potential of microwave-assisted processes: from synthesis of high-quality MIL-101 (fe) catalyst to furfural valorization. Appl. Mater. Today **39**, 102266 (2024)
53. A.M.P. Peedikakkal, I.H. Aljundi, Mixed-metal Cu-BTC metal–organic frameworks as a strong adsorbent for molecular hydrogen at low temperatures. ACS Omega **5**, 28493–28499 (2020)
54. V. Tzitzios, N. Kostoglou, M. Giannouri, G. Basina, C. Tampaxis, G. Charalambopoulou, T. Steriotis, K. Polychronopoulou, C. Doumanidis, C. Mitterer, Solvothermal synthesis, nanostructural characterization and gas cryo-adsorption studies in a metal–organic framework (IRMOF-1) material. Int. J. Hydrog. Energy. **42**, 23899–23907 (2017)
55. N.R. Habib, I. Diaz, A.M. Taddesse, H.W. Langmi, Selected sustainably synthesized metal–organic frameworks for hydrogen and carbon dioxide storage. Mater. Adv. (2026). https://doi.org/10.1039/d5ma00763a
56. D. Yuan, D. Zhao, D. Sun, H.C. Zhou, An isoreticular series of metal–organic frameworks with dendritic hexacarboxylate ligands and exceptionally high gas-uptake capacity. Angew. Chem. **122**, 5485–5489 (2010)
57. A. Morsali, L. Hashemi, *Nanoscale coordination polymers: preparation, function and application, advances in inorganic chemistry* (Elsevier, Amsterdam, 2020), pp.33–72
58. D.P. Broom, M. Hirscher, Irreproducibility in hydrogen storage material research. Energy & Environmental Science **9**, 3368–3380 (2016)
59. L.J. Murray, M. Dincă, J.R. Long, Hydrogen storage in metal–organic frameworks. Chem. Soc. Rev. **38**, 1294–1314 (2009)
60. H.W. Langmi, J. Ren, B. North, M. Mathe, D. Bessarabov, Hydrogen storage in metal-organic frameworks: a review. Electrochim. Acta **128**, 368–392 (2014)